Direct ink writing of porous shape memory polyesters†

Greeshma Raghuvaran,[a] Brandon M. Nitschke, [iD][b] Courteney T. Roberts,[b]
Melissa A. Grunlan [iD][abc] and Emily Pentzer [iD][*ac]

In this study, the direct ink write (DIW) additive manufacturing technique is employed to print "self-fitting" shape memory polymer (SMP) scaffolds with requisite porosity from biodegradable poly(ε-caprolactone)-diacrylate (PCL-DA)-based polymers. In contrast to cast systems, printing gives flexibility to produce scaffolds with macropores through print design, as well as bespoke geometry. Notably, the efficiency of bone scaffold implants in treating critically sized bone defects is highly dependent on conformal fit for osseointegration, and pore features for osteoinductivity. To create a suitable DIW ink, $\sim$40 wt% of salt particles (NaCl, <38 microns in diameter) were added to a polymer solution, endowing rheological properties required for printing- *i.e.*, shear thinning behavior and thixotropy. The prepared ink exhibited a drop in viscosity by 2 orders of magnitude with a shear rate increase of 3 orders of magnitude, alongside thixotropy evidenced by a 50% drop in viscosity upon a 100% shear rate change, reverting upon rate normalization. After printing, inks were cured *via* UV light-induced cross-linking of the polymer, then the structures washed with water to remove the salt and impart microporosity; thus, the salt particles served as sacrificial rheological modifiers. The final printed structures consisted of macropores that ranged from 200–300 microns with uniformly distributed $\sim$10–30 micron sized micropores. Notably, degradation studies revealed a progressive increase in degradation over time, with 73% mass loss after 15 days in 0.2 M aqueous sodium hydroxide. The composition, microstructure, thermal stability, degradation, and shape memory properties of the printed and cured objects are reported. This study gives insight into the DIW printing of these polymers, as relevant to customizable bone scaffolds, and examines the ink composition to understand the effects of different factors on the properties of the printed objects.

1. Introduction

Scaffolds useful for the treatment of bone defects require conformal fitting for osseointegration with surrounding bone tissue, as well as osteoinductivity imparted by requisite porosity and biodegradability.[1–4] The irregular geometries of bone defects necessitate tedious (and sometimes unsuccessful) fitting processes of harvested autografts, or the use of *in situ* curing fillers (*e.g.*, brittle bone cements).[5] In a regenerative approach, biodegradable, thermoresponsive shape memory polymer (SMP) scaffolds[6–8] with the capacity to self-fit within irregular bone defects[9] have been used. Macroporous SMP scaffolds (average pore size $\sim$200 μm) were previously prepared from poly(ε-caprolactone)-diacrylate (PCL-DA) *via* a solvent cast particulate leaching (SCPL)

technique.[10] In this process, a solution containing PCL-DA and photoinitiator were cast *via* centrifugation over a fused salt template, and subsequently UV-cured. The solvent was then evaporated, and the salt was extracted by soaking in a water/EtOH solution. When the scaffold was heated above its transition temperature ($T > T_{\text{trans}}$) (*i.e.*, the melt transition [T_{m}] of the PCL; $\sim$55 °C), it became malleable. Thus, the scaffold could be press-fit into an irregularly shaped defect, with shape recovery driving its expansion to the defect perimeter. Upon cooling to body temperature (37 °C, $T < T_{\text{trans}}$), the scaffold undergoes shape fixity within the defect. These SMP scaffolds have demonstrated utility in bone tissue regeneration,[11] both *in vitro*[9,12] and *in vivo*.[13] However, the SCPL technique is limited by lengthy fabrication times, as well as the inability to create scaffolds of larger and various sizes or control pore features.[14] Thus, a fabrication process that is inherently more flexible in creating desirable SMP scaffolds would be immensely useful.

Direct ink writing (DIW) is a widely utilized method of 3D printing based on the room temperature extrusion of an 'ink'.[15,16] The requirements for a suitable ink include thixotropic behavior, and the ability to be cured after printing. DIW

a Department of Materials Science and Engineering, Texas A&M University, College Station, TX 77843, USA. E-mail: emilypentzer@tamu.edu; Tel: +1 979 458 6688

b Department of Biomedical Engineering, Texas A&M University, College Station, TX 77843, USA. E-mail: mgrunlan@tamu.edu; Tel: +1 979 845 2406

c Department of Chemistry, Texas A&M University, College Station, TX 77843, USA

† Electronic supplementary information (ESI) available. See DOI: https://doi.org/10.1039/d4ma00137k

does not necessitate added heat, extending its suitability to temperature-sensitive materials,[17–19] including some that can provide desirable rheological modification[20,21] as well as induced porosity.[22,23] For example, Cipriani *et al.* created a DIW ink based on paraffin wax beads and a photocurable resin wherein the wax could be removed after printing/curing by washing with ethyl acetate, thereby generating pores.[24,25] Wei *et al.* showcased DIW inks based on sodium chloride (NaCl) particles combined with solvent-based solutions of triblock copolycarbonates, with porosity created upon washing with water to both cure the ink and remove the salt.[26] Thus, DIW with sacrificial fillers within the ink provides an opportunity to achieve both requisite rheology, and printed structures with multi-level porosity.[27]

The use of a DIW ink based on a SMP introduces a fourth dimension to conventional 3D printing techniques.[28] Referred to as '4D printing,' these printed objects undergo transformative changes over time.[29] For instance, Chen *et al.* produced 4D printed SMP structures *via* UV-assisted DIW printing of thermally cured epoxy composites.[30] Porous 4D printing systems have also been reported as dynamically evolving structures.[31–33] In a study by Kashyap *et al.*, 4D printing was employed to create shape memory polyurethanes (SMPUs) as self-deploying endovascular embolization devices by a combination of extrusion, fused filament fabrication, and salt leaching methods.[34] Herein, we report the development of an ink for DIW and printing to create 4D printed, biodegradable SMP structures with multi-level porosity. The ink was comprised of a solution of UV-curable PCL-DA and NaCl particles (Fig. 1). The ink displayed thixotropic behavior, permitting extrusion from a nozzle, and retention of filament shape which could undergo crosslinking *via* UV-curing. Subsequent washing with water removed both the solvent and salt particles, thereby imparting porosity. In this way, the salt particles served as both a rheology modifier and a sacrificial porogen. The composition, mechanical properties, shape memory behavior, and degradation of the printed SMP structures are reported and will guide further studies on the application of these bespoke structures.

2. Experimental details

Materials

PCL-DA (10k g mol^{-1}) was synthesized as previously reported.[9] The following chemicals were used as received, without further purification: *N*,*N*-dimethylformamide (DMF, Fisher), 2,2-dimethoxy-2-phenylacetophenone (DMP, TCI chemicals), chloroform (Supelco), dichloromethane (DCM, Sigma-Aldrich), and tetrahydrofuran (THF, JT Baker). Sodium chloride (NaCl, Fisher) was ground into small particles using an electric coffee grinder for $\sim$3 min. To ensure uniform particle size, the ground powder was sieved using a 400 US mesh number sieve and the particles that passed through were collected and used for ink development ($<$38 μm).

Instrumentation

DIW printing was conducted using a Hyrel 3D Engine SR equipped with an SDS-10 syringe extrusion head. Fourier transform infrared spectroscopy (FTIR) measurements were performed

Fig. 1 DIW process to prepare biodegradable, SMP 4D printed structures using a cross-linkable polyester-based ink in which salt particles were used as a rheology modifier and sacrificial porogen.

using a Jasco FT/IR-4600 Spectrometer with a diamond crystal on ZnSe ATR accessory. Scanning electron microscopy (SEM) images were captured using a TESCAN VEGA SEM at an accelerating voltage of 10 kV. Prior to imaging, SEM samples were sputter coated with 5 nm of Au. Energy dispersive X-ray spectroscopy (EDS) measurements were obtained using a JEOL JSM-7500F microscope equipped with an Oxford EDS system, which allowed for X-ray mapping and digital imaging. Thermogravimetric analysis (TGA) was conducted using a TA Instruments TGA 5500 instrument under a nitrogen (N$_2$) atmosphere. Differential scanning calorimetry (DSC) was performed using a TA Instruments DSC 2500 with a heating ramp of 5 °C min^{-1} over a temperature range of 0 °C to 100 °C. Tzero Aluminum pans were utilized for the DSC measurements. Rheological properties were analyzed using a TA Instruments DHR-2 Rheometer with a 25 mm parallel plate. Degradation studies were conducted with the help of VWR Benchtop Shaking Incubator Model 1570.

Ink formulation

PCL-DA was dissolved in a mixture of DMF and CHCl$_3$ to create the ink (see Table 1). A photoinitiator, DMP, was added to the mixture at an equivalent weight ratio of 5% of the polymer. Then, NaCl particles were incorporated into the mixture using a

Table 1 Ink composition for DIW of PCL-DA

PCL-DA	0.5 g
NaCl	1.25 g
DMF	0.6 mL
CHCl$_3$	0.3 mL
DMP	25 mg

Table 2 DIW print parameters

Nozzle	22G (0.413 ± 0.019 mm diameter)
Layer height	0.2 mm
Skirt	1 layer, 1 loop, 4 mm from object
Perimeter	1 layer
Horizontal/vertical shells	5
Print speed, travel speed	2 mm min^{-1}
Estimated printing time	6 min 58 s
Infill pattern, %	Rectilinear, 15%

Thinky mixer, which operated at the maximum rotational speed for 2 min at ambient temperature. The expected porosity in the printed structures was calculated by dividing the weight of NaCl by the combined weight of NaCl and PCL-DA. The solvents used in the ink formulation process were not included in the porosity calculation, as they were expected to be completely removed. From Table 1, this accounts for 1.25 grams in 1.5 grams, leading to an expected porosity of $\sim 71\%$.[35] This expected porosity matches cancellous bone which has a porosity between 70–85%, and can facilitate cell infiltration into the scaffold post-implantation.[36–39]

Direct ink writing (DIW)

The G-code for printing and curing operations was generated using Prusaslicer, which incorporates various parameters to determine the print output and design. The specific parameters employed for printing the optimal scaffold are shown in Table 2. To ensure smooth printing and eliminate initial extrusion irregularities, a skirt is first printed around the desired design. The skirt is later detached from the actual design and discarded. To minimize ink waste, the skirt is only printed in the first 1–2 layers and was omitted in subsequent runs. The printing process began with the puck's perimeter, followed by the infill pattern. The G-code takes care of curing each layer post-printing before moving on to subsequent layers. Next, to remove NaCl, the pucks were immersed in a beaker filled with 200 mL of deionized (DI) water containing ~ 2 mL of THF, and then stirred with a Teflon-covered stir bar at 300–400 rpm. The addition of THF to the DI water was found to expedite this salt removal. To validate the successful curing of the prints, each printed structure was immersed in a sealed vial containing 10 ml of DCM for 48 h at 200 rpm using a tabletop shaker. In this way, printed structures were generated with macropores sized 200–300 μm (distance between struts) and micropores sized 20–30 μm (*i.e.*, pore size created by salt porogen).

Rheometry

Rheology measurements were conducted to analyze the viscosity, modulus, and thixotropy properties of both the polymer solution (without salt) and the ink (with salt). Viscosity measurements were performed at shear rates from 10^{-3} to 10^3 s^{-1}. Initial data points obtained at lower shear rates were excluded from the analysis as they represented the time required for the instrument to stabilize and generate consistent data. Modulus measurements involved subjecting the samples to oscillation stress ranging from 10^{-3} to 10^3 Pa to evaluate variations in storage (G') and loss (G'') modulus with increasing strain. Thixotropy measurements involved monitoring the viscosity

of the samples over time while varying the shear rate in three steps: 0.5 s^{-1} for 720 s, followed by 1.0 s^{-1} for 60 s, and then returning to 0.5 s^{-1} for 240 s. To conduct the rheology measurements, the upper parallel plate of the rheometer was raised to a loading height of 8 cm, and approximately 1.2 mL of the polymer solution or ink was dispensed onto the lower plate. The upper plate was then lowered to a height equivalent to 1020 μm, and any excess sample was carefully removed from the plate's sides using a cotton swab. The upper plate was then lowered to establish a consistent 1000 μm gap, which was maintained throughout all experiments. The presented results represent the average data obtained from three sets that exhibited agreement with each other.

Degradation studies

The degradation of the printed and cured structures was assessed under base-catalyzed conditions by immersing them in a 0.2 M NaOH aqueous solution according to ASTM F1635. Printed structures (each weighing between 11 to 16 mg) were each submerged in 10 mL of the basic solution in a sealed glass vial and maintained in an incubator (37 °C and 60 rpm) for varying amounts of time. A total of 15 samples were used for the study, an average of 3 specimen mass reported for 5 different time points. At designated time points, the samples were taken out of the solution, dried under reduced pressure, and weighed to determine the extent of degradation. The presented weight measurement results were used to calculate the degradation percentage.

3. Results and discussion

Ink composition

The optimized ink for DIW of PCL-DA SMPs was developed through trial-and-error approach by varying solvent, polymer concentration, and loading of salt particles (<38 μm), using prior reports as guidance (Table 1).[15,24,26] We identified that salt particle loading should be ~ 40 wt% to impart thixotropic rheological behavior within a shear rate of 10^0 to 10^3 s^{-1}.[24] DMF and chloroform were selected as solvents as they fulfilled a number of criteria, including insolubility of salt and sufficient resistance to evaporation. At the desired PCL-DA concentration, we identified that a 1:2 ratio of chloroform to DMF could completely dissolve the polymer. Another critical component of the ink is incorporation of a photoinitiator for subsequent UV curing; loading of the photoinitiator (DMP) was varied, and 5 wt% (relative to polymer) was identified as giving appropriate shape memory properties, as lower concentrations led to

polymer dissolution after curing, and higher concentrations led to rigid structures *via* overcuring.

Rheology measurements

A DIW ink must exhibit thixotropic behavior, ensuring fluidification through a syringe yet stiffening at rest to maintain printed shape.[15,40] The rheological properties of the polymer solution (without salt) and ink (with salt) were assessed. As expected, the polymer solution exhibited Newtonian behavior, maintaining a consistent viscosity (100–200 mPa s) across different shear rates. In contrast, owing to the NaCl particles, the ink demonstrated shear-thinning behavior, with a decrease in viscosity from 10^5 to 10^3 mPa s as shear rate increased from 10^0 to 10^3 s^{-1} (Fig. 2a). This is consistent with our previous studies which showed that upon addition of an appropriate amount of filler, the ink exhibits a viscosity in the range of 10^5 to 10^6 at 10^0 shear rate.[24] The stress-dependent modulus analysis further confirmed the suitability of the ink for DIW printing (Fig. 2b). The polymer solution exhibited liquid-like behavior, with the loss modulus (G'') exceeding the storage modulus (G') at all stresses. In contrast, the ink exhibited a higher storage modulus (G') *versus* the loss modulus (G'') at low stresses, but a cross-over point occurred at $\sim$100 Pa. This observed yield stress suggests that the viscoelastic ink would favorably transition from a solid-like state at rest (*i.e.*, in the syringe and post-extrusion) to a liquid-like state upon extrusion. Finally, a thixotropic analysis was conducted (Fig. 2c). The viscosity of the polymer solution remained constant ($\sim$500 mPa s) regardless of shear rate, similar to its inherent viscosity. However, the ink exhibited a viscosity of $\sim 8 \times 10^4$ mPa s at a shear rate of 0.5 s^{-1}, which decreased to 4×10^4 mPa s when the shear rate was increased to 1.0 s^{-1}, then promptly returns to its original viscosity value when returned to a lower shear rate. Thus, the ink transitions from a solid-like state in the syringe, to a temporary liquid-like state during printing, then again to a solid-like state after leaving the nozzle. Overall, these results confirm that addition of salt particles are essential and effective in obtaining desirable rheological properties and a "printable" ink.

DIW printing

The print design was selected to represent a generalized scaffold that could be used to embed into and treat a bone defect. Printed specimens were prepared with a cylindrical base structure ($\sim$6 mm diameter), and a 15% rectilinear infill pattern that may provide better distribution of mechanical stress. The nozzle distance governed macroporosity (*i.e.*, space between struts), and microporosity was imparted by the salt porogen. Such multi-level porosity was expected to aid in cellular and neotissue infiltration prior to degradation, critical to bone regeneration.[41–43] The optimal print design was generated using PrusaSlicer software (Fig. 3a). By optimizing the infill percentage and nozzle size parameters, macropores with a size of 200–300 μm were achieved.

A 22G nozzle with an inner diameter of 0.413 ± 0.019 mm was employed to print the ink (Fig. 3b). The printing process involved alternating between ink extrusion and curing using a UV pen (365 nm). After each layer was extruded, UV light was
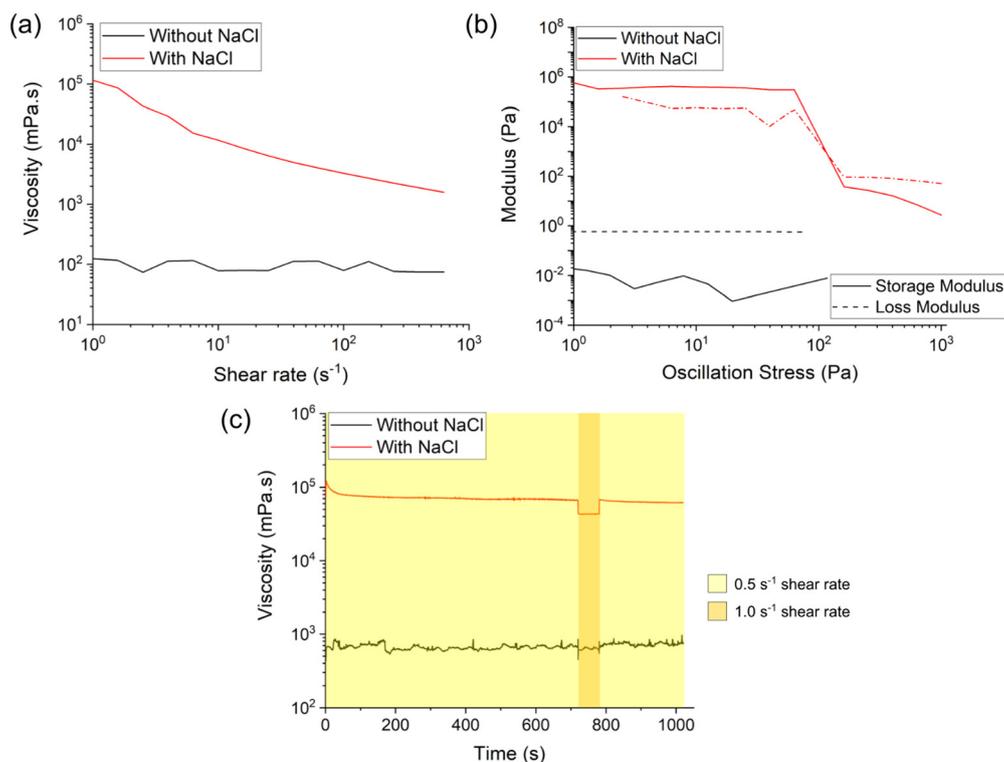
Fig. 2 Comparison of the properties of the polymer solution (no salt, black traces) and ink (with salt, red traces): (a) viscosity as a function of shear rate, (b) storage (G') and loss (G'') moduli variations *versus* applied stress, and (c) a three interval thixotropy test varying shear rate across time.
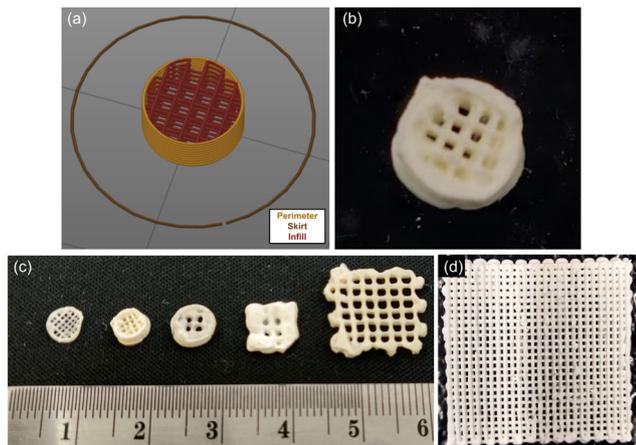
Fig. 3 DIW printing of shape memory inks and characterization after curing: (a) Prusaslicer design of scaffold, (b) DIW printed scaffold, (c) print nozzle-size-dependent macropore variation, and (d) 50 mm × 50 mm geometry print.

traced over the perimeter to initiate curing (*i.e.*, crosslinking of PCL-DA, Fig. S1, ESI†). The key parameters for the DIW prints are summarized in Table 2. Variations in nozzle sizes and print design sizes led to the production of different macropore sizes (from ~100 μm to ~1000 μm) (Fig. 3c). The scalability of the print is shown in Fig. 3d, with 50 × 50 mm scaffolds readily prepared.

Post-printing processes

After printing and UV-curing, the structures were annealed at 85 °C for an hour, as this step has previously been shown to enhance the shape memory properties of the cast structures.[15] The printed parts were then submerged in water which removed the solvent and salt particles, with the water replaced every 12 hours until a consistent mass was observed; we found that ~2% tetrahydrofuran (THF) expedites removal of salt particles from the inner pores by swelling the cross-linked polymer. Comparing the weight of the dried printed pucks post salt-removal to their weight pre-washing, the weight difference matched the theoretical value for salt removal (Table 2). Less than 10% shrinkage was observed in the printed samples upon drying, annealing, and washing.

FTIR spectroscopy was used to characterize the ink, "as printed" structures (*i.e.*, with salt), and final structures (*i.e.*, salt removed). The C=C stretching peaks (1669 cm^{-1}) and C=C bending peak (665 cm^{-1}) were present in the FTIR spectrum of the ink, but not for the "as printed" and final structures (Fig. S2, ESI†). This supports that curing led to cross-linking of the acrylate groups *via* consumption of the C=C. Successful crosslinking of PCL-DA was further confirmed by exposing final printed structures to DCM, which can solubilize unreacted PCL-DA. Following immersion in DCM, samples lost <15 wt%, which corresponds to the level of uncured PCL-DA in these printed structures and indicating the reasonable efficacy of UV-curing of the extruded inks.

Porosity

To confirm salt removal and the formation of pores within the printed struts, scanning electron microscopy (SEM) imaging and energy dispersive X-ray spectroscopy (EDS) analysis were conducted. Printed cross-sectional samples were prepared before and after salt removal. Cross-sectioned samples were prepared by freezing the pucks in liquid nitrogen prior to slicing, thereby avoid sample deformation. SEM images of the printed structures before salt removal clearly showed uniformly distributed salt particles tens of μm in size (Fig. 4a and b). After salt removal, the cross-section contains consistent pores with similar diameters to the salt particles (Fig. 4d and e). Complementary EDS results
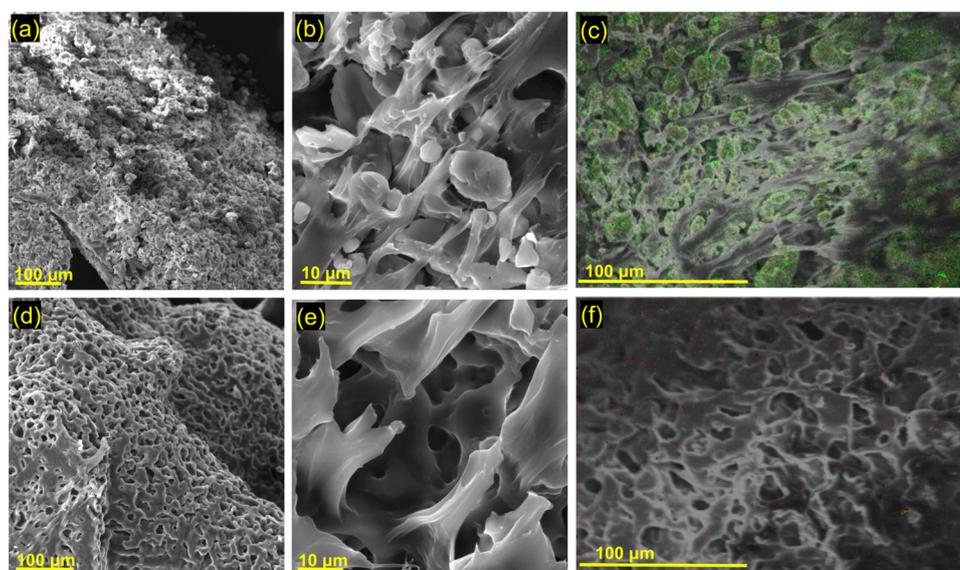
Fig. 4 SEM images of printed and cured samples: (a)–(c) before NaCl removal, and (d)–(f) after NaCl removal. (c) and (f) EDS mapping on SEM images (green = chlorine).
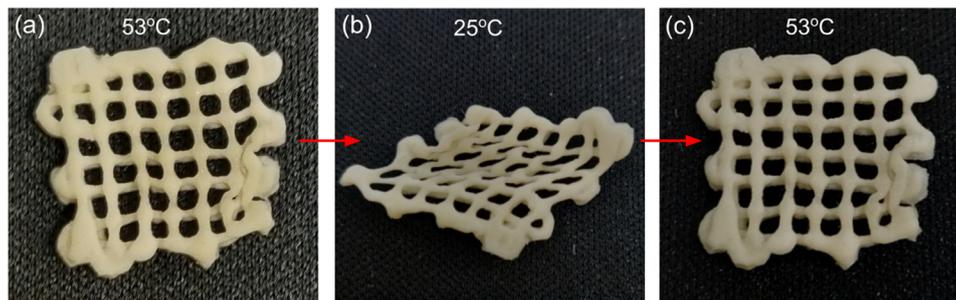
Fig. 5 Shape memory behavior of DIW printed PCL scaffolds: (a) sample after printing, curing, and washing; (b) shape fixity: sample in (a) after being heated to and deformed at 53 °C, then cooled to ambient tempeature; and (c) shape recovery of sample in (b) after heating at 53 °C.

before and after salt removal (Fig. 4c and f) confirm the absence of salt in the latter (*i.e.*, no chloride).

Thermal and shape memory properties

The thermogravimentic analysis (TGA) weight loss profile of the printed, cured, and washed structures reveals a single-step decomposition occurring at ~ 400 °C, which aligns with the expected thermal behavior of cross-linked PCL-DA (Fig. S3a, ESI†). The printed structures were also subjected to differential scanning calorimetry (DSC). The DSC analysis of the processed printed structure revealed a melting point of 53 °C, depicted in Fig. S3b (ESI†), consistent with that of PCL-DA. These findings again support that the printing process does not significantly alter the thermal stability or thermal properties of the polymer, supporting that the shape memory properties will be possible.

To assess the shape memory properties of the structures, a printed lattice was heated above the melting transition temperature of ~ 53 °C. Above this temperature, the sample softened, was deformed, then immersed in cold water to fix this new configuration. After removing the sample from cold water, the altered structure was maintained; however, subsequent heating above 53 °C restored the original lattice structure. Fig. 5a and b illustrate the stretching and twisting applied to a DIW PCL-DA lattice structure, as well as its subsequent shape recovery when exposed to its transformation temperature. This demonstrates the ability of the structures to "remember" an initial configuration and exhibit shape recovery under the appropriate conditions.

Degradation studies

For bone scaffolds, the controlled degradation of implants is essential as it promotes osteointegration and bone regeneration with time. To assess the degradation behavior, nine scaffolds were immersed in an aqueous solution of 0.2 M NaOH.

The alkaline nature of NaOH accelerates the hydrolysis of ester bonds in the polymer network of the scaffolds, facilitating a base-catalyzed mode of degradation. This degradation testing method provides valuable insights into the scaffold's performance, aiding in the development of more effective biomaterials for regenerative engineering applications. The weight difference at different immersion periods within each set was used to calculate the degradation percentage for each sample. The degradation studies revealed a progressive increase in degradation over time, with degradation percentages of 4% on day 3, 13% on day 6, 29% on day 9, 45% on day 12, and reaching 73% on day 15. The average degradation percentages for each sample at different time points are summarized in Table 3, with the associated mass loss represented in Fig. 6 (raw data for the calculations can be found in Table S1, ESI†). Notably, previous studies of the degradation of porous PCL structures under similar conditions demonstrated slightly faster degradation rates (*e.g.*, ~ 50 wt% loss after 7 days[44]); however, these were created using different fabrication methods which led to differences in pore structure and surface area. For reference, degradation of solid PCL takes ~ 2 years in non-accelerated conditions but for tissue engineering and ideal

Table 3 Degradation studies

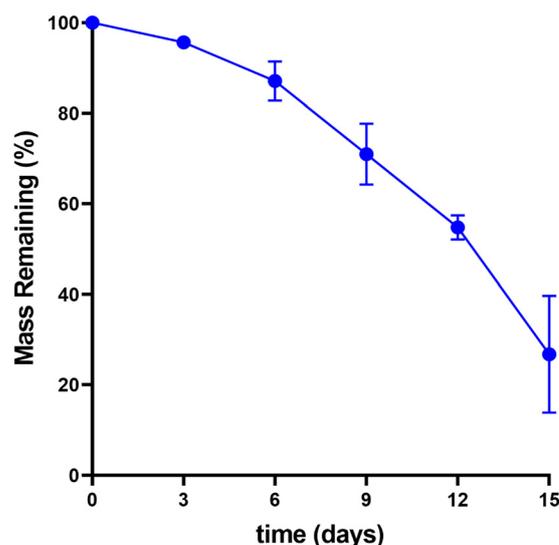| Number of days	Average deg. %	Standard deviation
3	4.334	0.605
6	12.898	4.320
9	29.043	6.749
12	45.221	2.666
15	73.252	12.924

Fig. 6 Mass loss of accelerated degradation (0.2 M NaOH) study.

scaffold would degrade at the same rate as bone tissue formation (*i.e.*, 3–6 months).[45] These findings indicate that the printed scaffolds could potentially degrade under conditions appropriate for clinical efficacy.

4. Conclusions

In this study, we develop a composite ink and use direct ink write printing to produce porous shape memory polymers with potential applications as bone scaffolds. Sacrificial NaCl particles serve as porogens and were added to a solution of PCL-DA and photoinitiator to create an ink that could be printed by DIW then cured with UV light. The rheological properties of the inks, as relevant to printing, were characterized (shear thinning, yield stress, and thixotropy) and different gauged needs were demonstrated useful. After printing, UV light was used to cross-link the polymer, then the structure was washed with water to remove solvent and salt, thereby producing a porous structure with shape memory properties. Thus, salt particles are used to access appropriate rheological behavior as well as to endow porosity to the final structure. Processing by printing, rather than casting, allows for cylindrical scaffolds with suitable filler sizes and layer heights to be prepared which contain both macropores (from printing) and micropores (from salt removal). Future improvements in ink formulation will focus on using "greener" solvents and evaluating osteoinductive properties. Furthermore, more complex geometries could be explored to achieve macropores or non-sacrificial fillers, such as liquid-filled capsules which would enable delivery of nutrients or biological reagents as the scaffold degrades within the body.[46]

Author contributions

M. G. and E. P. conceived the research and defined goals. B. N. and C. R. synthesized PCL-DA for the studies and conducted the degradation studies. G. R. conducted the ink formulation, printing, and conducted measurements, as well as drafted the initial manuscript. E. P. supervised, advised, and acquired funding for the research. The manuscript was edited by all authors.

Conflicts of interest

There are no conflicts of interest to declare.

Acknowledgements

References

1 T. Albrektsson and C. Johansson, Osteoinduction, Osteo-conduction and Osseointegration, *Eur. Spine J.*, 2001, **10**(2), S96–S101, DOI: **10.1007/s005860100282**.

2 P. X. Ma and J. Elisseeff, *Scaffolding in Tissue Engineering*, CRC Press, 2005.

3 A. H. Foroughi and M. J. Razavi, Multi-Objective Shape Optimization of Bone Scaffolds: Enhancement of Mechanical Properties and Permeability, *Acta Biomater.*, 2022, **146**, 317–340, DOI: **10.1016/j.actbio.2022.04.051**.

4 Y. Zuo, W. Xiao, X. Chen, Y. Tang, H. Luo and H. Fan, Bottom-up Approach to Build Osteon-like Structure by Cell-Laden Photocrosslinkable Hydrogel, *Chem. Commun.*, 2012, **48**(26), 3170, DOI: **10.1039/c2cc16744a**.

5 E. Neovius and T. Engstrand, Craniofacial Reconstruction with Bone and Biomaterials: Review over the Last 11 Years, *J. Plast. Reconstr. Aesthet. Surg.*, 2010, **63**(10), 1615–1623, DOI: **10.1016/j.bjps.2009.06.003**.

6 L. Sun, W. M. Huang, Z. Ding, Y. Zhao, C. C. Wang, H. Purnawali and C. Tang, Stimulus-Responsive Shape Memory Materials: A Review, *Mater. Des.*, 2012, **33**, 577–640, DOI: **10.1016/j.matdes.2011.04.065**.

7 Polymers | Free Full-Text | Advanced Shape Memory Technology to Reshape Product Design, Manufacturing and Recycling. **https://www.mdpi.com/2073-4360/6/8/2287** (accessed 2023-06-20).

8 A. Kirillova and L. Ionov, Shape-Changing Polymers for Biomedical Applications, *J. Mater. Chem. B*, 2019, **7**(10), 1597–1624, DOI: **10.1039/C8TB02579G**.

9 D. Zhang, O. J. George, K. M. Petersen, A. C. Jimenez-Vergara, M. S. Hahn and M. A. Grunlan, A Bioactive "Self-Fitting" Shape Memory Polymer Scaffold with Potential to Treat Cranio-Maxillo Facial Bone Defects, *Acta Biomater.*, 2014, **10**(11), 4597–4605, DOI: **10.1016/j.actbio.2014.07.020**.

10 L. N. Nail, D. Zhang, J. L. Reinhard and M. A. Grunlan, Fabrication of a Bioactive, PCL-Based "Self-Fitting" Shape Memory Polymer Scaffold, *J. Visualized Exp.*, 2015, **104**, 52981, DOI: **10.3791/52981**.

11 M. R. Pfau and M. A. Grunlan, Smart Scaffolds: Shape Memory Polymers (SMPs) in Tissue Engineering, *J. Mater. Chem. B*, 2021, **9**(21), 4287–4297, DOI: **10.1039/D1TB00607J**.

12 J. M. Stukel Shah, B. Lundquist, J. Macaitis, M. R. Pfau-Cloud, F. O. Beltran, M. A. Grunlan, W. Lien, H. Wang and A. J. Burdette, Comparative Evaluation of Mesenchymal Stromal Cell Growth and Osteogenic Differentiation on a Shape Memory Polymer Scaffold, *J. Biomed. Mater. Res., Part B*, 2022, **110**(9), 2063–2074, DOI: **10.1002/jbm.b.35061**.

13 M. R. Pfau, F. O. Beltran, L. N. Woodard, L. K. Dobson, S. B. Gasson, A. B. Robbins, Z. T. Lawson, W. Brian Saunders, M. R. Moreno and M. A. Grunlan, Evaluation of a Self-Fitting, Shape Memory Polymer Scaffold in a Rabbit Calvarial Defect Model, *Acta Biomater.*, 2021, **136**, 233–242, DOI: **10.1016/j.actbio.2021.09.041**.

14 J. M. Karp, K. Rzeszutek, M. S. Shoichet and J. E. Davies, Fabrication of Precise Cylindrical Three-Dimensional

Tissue Engineering Scaffolds for In Vitro and In Vivo Bone Engineering Applications, *J. Craniofac. Surg.*, 2003, **14**(3), 317.

15 P. Wei, C. Cipriani, C.-M. Hsieh, K. Kamani, S. Rogers and E. Pentzer, Go with the Flow: Rheological Requirements for Direct Ink Write Printability, *J. Appl. Phys.*, 2023, **134**(10), 100701, DOI: **10.1063/5.0155896**.

16 D. A. Rau, M. J. Bortner and C. B. Williams, A Rheology Roadmap for Evaluating the Printability of Material Extrusion Inks, *Addit. Manuf.*, 2023, **75**, 103745, DOI: **10.1016/j.addma.2023.103745**.

17 H. Baniasadi, R. Ajdary, J. Trifol, O. J. Rojas and J. Seppälä, Direct Ink Writing of Aloe Vera/Cellulose Nanofibrils Bio-Hydrogels, *Carbohydr. Polym.*, 2021, **266**, 118114, DOI: **10.1016/j.carbpol.2021.118114**.

18 E. A. Guzzi, R. Bischof, D. Dranseikiene, D. V. Deshmukh, A. Wahlsten, G. Bovone, S. Bernhard and M. W. Tibbitt, Hierarchical Biomaterials via Photopatterning-Enhanced Direct Ink Writing, *Biofabrication*, 2021, **13**(4), 044105, DOI: **10.1088/1758-5090/ac212f**.

19 R. Ajdary, G. Reyes, J. Kuula, E. Raussi-Lehto, T. S. Mikkola, E. Kankuri and O. J. Rojas, Direct Ink Writing of Biocompatible Nanocellulose and Chitosan Hydrogels for Implant Mesh Matrices, *ACS Polym. Au*, 2022, **2**(2), 97–107, DOI: **10.1021/acspolymersau.1c00045**.

20 C. P. Lee, R. Karyappa and M. Hashimoto, 3D Printing of Milk-Based Product, *RSC Adv.*, 2020, **10**(50), 29821–29828, DOI: **10.1039/D0RA05035K**.

21 M. Zuo, N. Pan, Q. Liu, X. Ren, Y. Liu and T.-S. Huang, Three-Dimensionally Printed Polylactic Acid/Cellulose Acetate Scaffolds with Antimicrobial Effect, *RSC Adv.*, 2020, **10**(5), 2952–2958, DOI: **10.1039/C9RA08916K**.

22 S. Tajik, C. N. Garcia, S. Gillooley and L. Tayebi, 3D Printing of Hybrid-Hydrogel Materials for Tissue Engineering: A Critical Review, *Regener. Eng. Transl. Med.*, 2023, **9**(1), 29–41, DOI: **10.1007/s40883-022-00267-w**.

23 Y. Lin, R. Yang and X. Wu, Recent Progress in the Development of Conductive Hydrogels and the Application in 3D Printed Wearable Sensors, *RSC Appl. Polym.*, 2023, **1**(2), 132–157, DOI: **10.1039/D3LP00077J**.

24 C. E. Cipriani, T. Ha, O. B. Martinez Defilló, M. Myneni, Y. Wang, C. C. Benjamin, J. Wang, E. B. Pentzer and P. Wei, Structure–Processing–Property Relationships of 3D Printed Porous Polymeric Materials, *ACS Mater. Au*, 2021, **1**(1), 69–80, DOI: **10.1021/acsmaterialsau.1c00017**.

25 P. Wei, C. E. Cipriani and E. B. Pentzer, Thermal Energy Regulation with 3D Printed Polymer-Phase Change Material Composites, *Matter*, 2021, **4**(6), 1975–1989, DOI: **10.1016/j.matt.2021.03.019**.

26 P. Wei, G. A. Bhat, C. E. Cipriani, H. Mohammad, K. Schoonover, E. B. Pentzer and D. J. Darensbourg, 3D Printed CO2-Based Triblock Copolymers and Post-Printing Modification, *Angew. Chem., Int. Ed.*, 2022, **61**(37), e202208355, DOI: **10.1002/anie.202208355**.

27 M. Farid, A. Purniawan, D. Susanti, A. Rasyida, H. Yulianto and M. Ramadani, Effect of Nanocellulose on Acoustical

and Thermal Insulation Properties of Silicone Rubber Composite, *Mater. Sci. Forum*, 2019, **964**, 156–160, DOI: **10.4028/www.scientific.net/MSF.964.156**.

28 L. Halbardier, E. Goldbach, C. Croutxé-Barghorn, A.-S. Schuller and X. Allonas, Combined Aza-Michael and Radical Photopolymerization Reactions for Enhanced Mechanical Properties of 3D Printed Shape Memory Polymers, *RSC Adv.*, 2022, **12**(47), 30381–30385, DOI: **10.1039/D2RA05404C**.

29 X. Wan, H. Wei, F. Zhang, Y. Liu and J. Leng, 3D Printing of Shape Memory Poly(d,l-Lactide-Co-Trimethylene Carbonate) by Direct Ink Writing for Shape-Changing Structures, *J. Appl. Polym. Sci.*, 2019, **136**(44), 48177, DOI: **10.1002/app.48177**.

30 K. Chen, X. Kuang, V. Li, G. Kang and H. J. Qi, Fabrication of Tough Epoxy with Shape Memory Effects by UV-Assisted Direct-Ink Write Printing, *Soft Matter*, 2018, **14**(10), 1879–1886, DOI: **10.1039/C7SM02362F**.

31 X. Mu, T. Bertron, C. Dunn, H. Qiao, J. Wu, Z. Zhao, C. Saldana and H. J. Qi, Porous Polymeric Materials by 3D Printing of Photocurable Resin, *Mater. Horiz.*, 2017, **4**(3), 442–449, DOI: **10.1039/C7MH00084G**.

32 F. S. Senatov, K. V. Niaza, M. Yu Zadorozhnyy, A. V. Maksimkin, S. D. Kaloshkin and Y. Z. Estrin, Mechanical Properties and Shape Memory Effect of 3D-Printed PLA-Based Porous Scaffolds, *J. Mech. Behav. Biomed. Mater.*, 2016, **57**, 139–148, DOI: **10.1016/j.jmbbm.2015.11.036**.

33 K. Hearon, P. Singhal, J. Horn, W. Small, C. Olsovsky, K. C. Maitland, T. S. Wilson and D. J. Maitland, Porous Shape-Memory Polymers, *Polym. Rev.*, 2013, **53**(1), 41–75, DOI: **10.1080/15583724.2012.751399**.

34 D. Kashyap, P. Kishore Kumar and S. Kanagaraj, 4D Printed Porous Radiopaque Shape Memory Polyurethane for Endovascular Embolization, *Addit. Manuf.*, 2018, **24**, 687–695, DOI: **10.1016/j.addma.2018.04.009**.

35 J. Wei, J. Jia, F. Wu, S. Wei, H. Zhou, H. Zhang, J.-W. Shin and C. Liu, Hierarchically Microporous/Macroporous Scaffold of Magnesium–Calcium Phosphate for Bone Tissue Regeneration, *Biomaterials*, 2010, **31**(6), 1260–1269, DOI: **10.1016/j.biomaterials.2009.11.005**.

36 E. F. Morgan, G. U. Unnikrisnan and A. I. Hussein, Bone Mechanical Properties in Healthy and Diseased States, *Annu. Rev. Biomed. Eng.*, 2018, **20**, 119–143, DOI: **10.1146/annurev-bioeng-062117-121139**.

37 M. Prakasam, A. Chirazi, G. Pyka, A. Prokhodtseva, D. Lichau and A. Largeteau, Fabrication and Multiscale Structural Properties of Interconnected Porous Biomaterial for Tissue Engineering by Freeze Isostatic Pressure (FIP), *J. Funct. Biomater.*, 2018, **9**(3), 51, DOI: **10.3390/jfb9030051**.

38 J. Jiao, Q. Hong, D. Zhang, M. Wang, H. Tang, J. Yang, X. Qu and B. Yue, Influence of Porosity on Osteogenesis, Bone Growth and Osteointegration in Trabecular Tantalum Scaffolds Fabricated by Additive Manufacturing, *Front. Bioeng. Biotechnol.*, 2023, 11, DOI: **10.3389/fbioe.2023.1117954**.

39 S. J. Hollister, Porous Scaffold Design for Tissue Engineering, *Nat. Mater.*, 2005, **4**(7), 518–524, DOI: **10.1038/nmat1421**.

40 D. A. Rau, C. B. Williams and M. J. Bortner, Rheology and Printability: A Survey of Critical Relationships for Direct Ink

Write Materials Design, *Prog. Mater. Sci.*, 2023, **140**, 101188, DOI: **10.1016/j.pmatsci.2023.101188**.

41 B. Xu, K.-W. Lee, W. Li, M. J. Yaszemski, L. Lu, Y. Yang and S. Wang, A Comparative Study on Cylindrical and Spherical Models in Fabrication of Bone Tissue Engineering Scaffolds: Finite Element Simulation and Experiments, *Mater. Des.*, 2021, **211**, 110150, DOI: **10.1016/j.matdes.2021.110150**.

42 M. Deng, S. G. Kumbar, L. S. Nair, A. L. Weikel, H. R. Allcock and C. T. Laurencin, Biomimetic Structures: Biological Implications of Dipeptide-Substituted Polyphosphazene–Polyester Blend Nanofiber Matrices for Load-Bearing Bone Regeneration, *Adv. Funct. Mater.*, 2011, **21**(14), 2641–2651, DOI: **10.1002/adfm.201100275**.

43 H. Jiang, Y. Zuo, Q. Zou, H. Wang, J. Du, Y. Li and X. Yang, Biomimetic Spiral-Cylindrical Scaffold Based on Hybrid Chitosan/Cellulose/Nano-Hydroxyapatite Membrane for Bone Regeneration, *ACS Appl. Mater. Interfaces*, 2013, **5**(22), 12036–12044, DOI: **10.1021/am4038432**.

44 M. R. Pfau, K. G. McKinzey, A. A. Roth, L. M. Graul, D. J. Maitland and M. A. Grunlan, Shape Memory Polymer (SMP) Scaffolds with Improved Self-Fitting Properties, *J. Mater. Chem. B*, 2021, **9**(18), 3826–3837, DOI: **10.1039/D0TB02987D**.

45 S. Bose, M. Roy and A. Bandyopadhyay, Recent Advances in Bone Tissue Engineering Scaffolds, *Trends Biotechnol.*, 2012, **30**(10), 546–554, DOI: **10.1016/j.tibtech.2012.07.005**.

46 C. E. Cipriani, N. C. Starvaggi, K. J. Edgehouse, J. B. Price, S. L. Vivod and E. B. Pentzer, Additive Manufacturing: Modular Platform for 3D Printing Fluid-Containing Monoliths, *Mol. Syst. Des. Eng.*, 2022, **7**(9), 1039–1044, DOI: **10.1039/D2ME00102K**.